Structure of Spin-Labeled Methylmethanethiolsulfonate in Solution and Bound to TEM-1 β-Lactamase Determined by Electron Nuclear Double Resonance Spectroscopy†

Devkumar Mustafi,* Alejandro Sosa-Peinado,‡ Vanita Gupta, David J. Gordon, and Marvin W. Makinen

Department of Biochemistry and Molecular Biology, The University of Chicago, Cummings Life Science Center, 920 East 58th Street, Chicago, Illinois 60637

Received March 15, 2001; Revised Manuscript Received October 31, 2001

ABSTRACT: Site-directed spin-labeling of proteins whereby the spin-label methyl 3-(2,2,5,5-tetramethyl-1-oxypyrrolinyl)methanethiolsulfonate (SLMTS) is reacted with the −SH groups of cysteinyl residues incorporated into a protein by mutagenesis has been successfully applied to investigate secondary structure and conformational transitions of proteins. In these studies, it is expected that the spin-label moiety adopts different conformations dependent on its local environment. To determine the conformation of SLMTS in solution reacted with L-cysteine (SLMTCys) and bound in the active site of the Glu240Cys mutant of TEM-1 β-lactamase, we have synthesized SLMTS both of natural abundance isotope composition and in site-specifically deuterated forms for electron nuclear double resonance (ENDOR) studies. ENDOR-determined electron−proton distances from the unpaired electron of the nitroxyl group of the spin-label to the methylene and methyl protons of SLMTS showed three conformations of the oxypyrrolinyl ring with respect to rotation around the S−S bond dependent on the solvent dielectric constant. For SLMTCys, two conformations of the molecule were compatible with the ENDOR-determined electron−nucleus distances to the side-chain methylene protons and to H^{α} and $H^{\beta 1,2}$ of cysteine. To determine SLMTS conformation reacted with the Glu240Cys mutant of TEM-1 β-lactamase, enzyme was overexpressed in both ordinary and perdeuterated minimal medium. Resonance features of H^{α} and $H^{\beta 1,2}$ of the Cys240 residue of the mutant and of the side-chain methylene protons within the spin-label moiety yielded electron−proton distances that sterically accommodated the two conformations of free SLMTCys in solution.

Site-directed spin-labeling with the use of nitroxyl spin-labels has become a useful tool for determination of protein structure and dynamics (*1*−*9*). Nitroxyl spin-labels are stable organic free radicals that can be strategically attached to biomolecules to provide detailed information of the local molecular environment through the application of electron paramagnetic resonance (EPR)[1] spectroscopy. Hubbell and co-workers and others have shown that analysis of the EPR spectra of nitroxyl spin-labels covalently attached to proteins provides valuable information to (i) determine topology, (ii) assign secondary structure, (iii) define the depth of residues from the membrane surface in a transmembrane helix, and (iv) monitor protein conformational changes (*1*−*9*). The general approach is to incorporate reactive cysteine residues into recombinant proteins by mutagenesis to provide points of attachment for the nitroxyl spin-label. Reaction of the spin-label methyl 3-(2,2,5,5-tetramethyl-1-oxypyrrolinyl)methanethiolsulfonate (SLMTS)[1] according to Scheme 1 is highly specific and is based on the specific reactivity of methylmethanethiolsulfonate to measure sulfhydryl content of proteins (*10*). It has been shown that the spin-label derivative reacts with both exposed and buried cysteine residues (*11*).

While spin-label mutagenesis has been employed hitherto only through application of EPR, the methodology could be extended further by applying electron nuclear double resonance (ENDOR)[1] spectroscopy. Recent studies, particularly from our laboratory, have demonstrated that ENDOR spectroscopy of spin-labels in frozen glassy solutions can be an incisive method to assign the relative coordinates of nearby magnetic nuclei with an accuracy that is not usually associated with molecules in solution (*12*−*23*). Because the unpaired electron of nitroxyl spin-labels behaves as an effective point dipole, located at about the midpoint of the N−O bond of the nitroxyl group (*15*), the hyperfine (hf)[1] interactions of nearby nuclei with the unpaired electron are largely dipole−dipole in character. We have shown that this hf coupling can be measured accurately by ENDOR to obtain electron−nucleus dipolar distances in the range of 3−11 Å with errors as low as 5% based on ENDOR line widths. In these studies, we have shown that ENDOR of nitroxyl spin-

† This work was supported by grants from the National Institutes of Health and the National Science Foundation. V.G. was supported in part by an HHMI undergraduate summer research fellowship and by an NSF REU award (MCB9513838), and D.J.G. was supported by an NIH MSTP training grant (GM07281).

* To whom correspondence should be addressed. Phone: (773) 702-1667. Fax: (773) 702-0439. E-mail: dmustafi@midway.uchicago.edu.

‡ Present address: Department of Biochemistry, School of Medicine, National Autonomous University of Mexico, Mexico D.F. 04510.

[1] Abbreviations: ENDOR, electron nuclear double resonance; EPR, electron paramagnetic resonance; MeOH, methanol; PIPES, piperazine-*N*, *N*′-bis[2-ethanesulfonic acid]; hf, hyperfine; hfc, hyperfine coupling; SLMTCys, *S*-[3-(2,2,5,5-tetramethyl-1-oxypyrrolinyl)methylthiol]-L-cysteine; SLMTS, methyl 3-(2,2,5,5-tetramethyl-1-oxypyrrolinyl)-methanethiolsulfonate.

10.1021/bi010539p CCC: $22.00
Published on Web 12/27/2001

Scheme 1

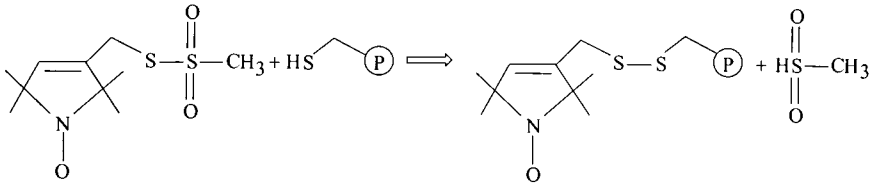

labels in combination with molecular modeling provides a general method for the determination of the structure and conformation of both small molecules and enzyme reaction intermediates in solution with a precision that is exceeded only by that of single-crystal X-ray diffraction (*12*−*23*).

Despite the usefulness of the SLMTS molecule as a structural probe, its molecular structure and conformation in solution have not yet been determined. Here, we describe the ENDOR-determined structure and conformation of SLMTS free in solution and reacted with L-cysteine. By application of angle-selected ENDOR, the hf couplings yield the relative coordinates of protons with respect to the unpaired electron of the nitroxyl spin-label. The ENDOR-determined distances are then used as constraints in torsion angle search calculations to define molecular conformation. From these investigations, we show that the ENDOR-determined electron−nucleus distances of SLMTS within van der Waals conformational space accommodate three conformations of the oxypyrrolinyl ring with respect to rotation around the S−S bond. While one of these conformers is unlikely to be populated and thereby probably represents only a mathematical solution to the conformational search, the relative populations of the two other conformers are dependent on solvent polarity. We also provide a detailed description of the three-dimensional ENDOR structures of SLMTS reacted with L-cysteine in solution and bound to the Cys240 residue in the active site of the Glu240Cys mutant of TEM-1 β-lactamase. The structure of the spin-labeled Glu240Cys mutant is particularly relevant in view of the recent X-ray description of SLMTS reacted with cysteine mutants of T4 lysozyme (*11*). Furthermore, the results of our ENDOR studies of nitroxyl spin-labels show that this method can be applied to problems requiring the precise determination of the detailed local structure of macromolecules in solution.

MATERIALS AND METHODS

General. The parent spin-label 2,2,5,5-tetramethyl-1-oxypyrroline-3-carboxylic acid was obtained by hydrolysis of 2,2,5,5-tetramethyl-1-oxypyrroline-3-carboxamide (Aldrich Chemical Co. Inc., Milwaukee, WI) according to the method of Rozantsev (*24*). Thionyl chloride, pyridine, triethylamine, lithium bromide, methanesulfonyl chloride, lithium aluminum hydride, lithium aluminum deuteride, and sodium sulfide were purchased from Aldrich. Lithium tris-(*tert*-butoxy)aluminum hydride [$LiAlH(O\text{-}t\text{Bu})_3$] and its deuterated analogue $LiAl^2H(O\text{-}t\text{Bu})_3$ were prepared immediately before use according to the procedure of Brown and Rao (*25*). Sodium methanethiolsulfonate ($NaS_2O_2CH_3$) was prepared from Na_2S and methanethiosulfonyl chloride and recrystallized three times with absolute ethanol according to the procedure of Kenyon and Bruice (*26*). THF was refluxed and distilled over $LiAlH_4$; $SOCl_2$, Et_3N, and pyridine were purified by distillation and stored over molecular sieves.

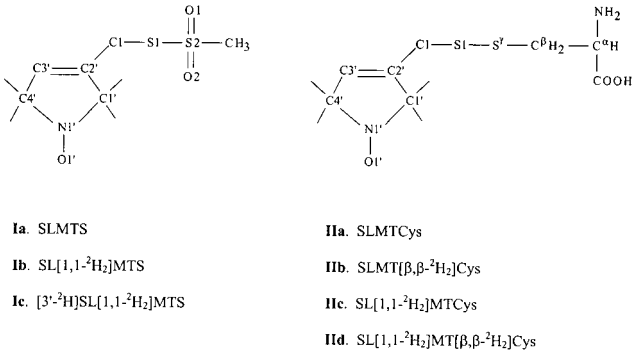

Ia. SLMTS

Ib. SL[1,1-$^2H_2$]MTS

Ic. [3′-^{2}H]SL[1,1-$^2H_2$]MTS

IIa. SLMTCys

IIb. SLMT[β,β-$^2H_2$]Cys

IIc. SL[1,1-$^2H_2$]MTCys

IId. SL[1,1-$^2H_2$]MT[β,β-$^2H_2$]Cys

FIGURE 1: Illustration of the chemical bonding structures and the atomic numbering schemes of methyl 3-(2,2,5,5-tetramethyl-1-oxypyrrolinyl)methanethiolsulfonate and *S*-[3-(2,2,5,5-tetramethyl-1-oxypyrrolinyl)methylthiol]-L-cysteine. Also shown are specifically deuterated analogues of SLMTS and SLMTCys employed in this study. SL refers to the spin-label acyl moiety attached to the methylene carbon C(1) atom.

L-Cysteine and D,L-[β,β-$^2H_2$]cysteine were purchased from Aldrich and Cambridge Isotope Laboratories, Inc. (Woburn, MA), respectively. Deuterated solvents (≥99% ^{2}H) were purchased from Cambridge Isotope Laboratories. All other reagents were of analytical reagent grade, and deionized distilled water was used throughout.

Methyl 3-(2,2,5,5-tetramethyl-1-oxypyrrolinyl)methanethiolsulfonate (***Ia***). In Figure 1 is illustrated the chemical bonding structure of the parent compound SLMTS (**Ia)** and of site-specifically deuterated analogues employed in this investigation. **Ia** was synthesized by adapting the previously published procedure of Berliner et al. (*27*). For brevity, we outline the synthesis in Scheme 2. Except for compounds **IB** and **IE** that were obtained as oils, all other reaction intermediates and products were recrystallized and characterized by melting point, mass spectra, and elemental analysis. Mass spectrometric analysis was carried out by Dr. Steven Mullen in the School of Chemical Sciences at the University of Illinois at Urbana-Champaign. Elemental composition was determined by Midwest Microlabs (Indianapolis, IN). Analytical data for compounds **Ia**−**c** are summarized in Table 1. According to Scheme 2, typical yields were as follows: compound **IC** (starting from **IA**), 57%; compound **ID** (from **IC**), 78%; and the final product **Ia** (from **ID**), 48%.

[$^2H_2$]Methyl 3-(2,2,5,5-tetramethyl-1-oxypyrrolinyl)methanethiolsulfonate (**Ib**) was synthesized according to the method for **Ia** except that the acid chloride (**IB**) was reduced with $LiAl^2H(O\text{-}t\text{Bu})_3$. No evidence of the presence of **Ia** was detected by mass spectrometric analysis of **Ib**.

[$^2H_2$]Methyl 3-(2,2,5,5-tetramethyl-1-oxy-[3′-^{2}H]pyrrolinyl)methanethiolsulfonate (**Ic**) was synthesized according to the method for **Ib** except that 2,2,5,5-tetramethyl-1-oxy-[3′-^{2}H]pyrroline-3-carboxylic acid was used in the first step. This deuterated analogue of the spin-label acid was synthesized according to Rozantsev (*24*) from 4-oxo-2,2,6,6-tetramethyl-

Scheme 2

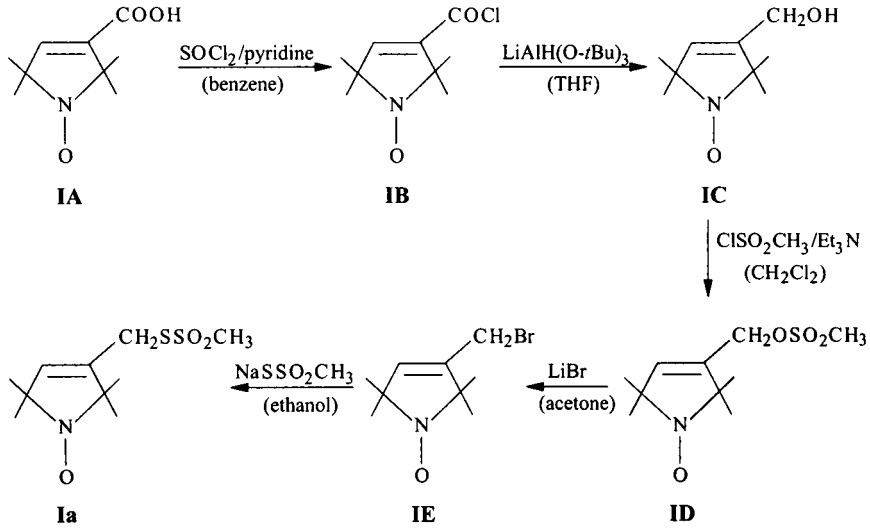

Table 1: Summary of Analytical Results Characterizing Methyl 3-(2,2,5,5-tetramethyl-1-oxypyrrolinyl)methanethiolsulfonate and Site-Specifically Deuterated Analogs

			elemental analysis: calculated (found)				
compound	chemical formula	melting point (°C)	C	H	N	S	*m/e*
Ia	$C_{10}H_{18}NO_3S_2$	106−107	45.43 (45.50)	6.86 (6.90)	5.30 (5.30)	24.25 (24.50)	264
Ib	$C_{10}H_{16}D_2NO_3S_2$	106.5−107	45.09 (45.06)	6.86 (6.76)	5.26 (5.34)	24.07 (23.96)	266
Ic	$C_{10}H_{15}D_3NO_3S_2$	106.5−107	44.92 (45.03)	6.86 (6.95)	5.24 (5.24)	23.98 (24.02)	267

piperidine monohydrate (Aldrich) using perdeuterated acetic acid, hydrobromic acid, and potassium hydroxide (*13*, *28*). No evidence of the presence of **Ia** or **Ib** was detected by mass spectrometric analysis of **Ic**.

S-[3-(2,2,5,5-Tetramethyl-1-oxypyrrolinyl)methylthiol]-L-cysteine (***IIa***). A solution of 200 mg (0.757 mmol) of **Ia** in 20 mL of acetone was added dropwise with vigorous stirring over a period of 15 min to a solution of 83 mg (0.688 mmol) of L-cysteine in 30 mL of water at 25 °C. The mixture was stirred for 3 h at 25 °C. The resulting solution was shaken with 15 mL of ether, and the ether layer was decanted. This procedure was repeated five times until the ether layer was colorless. TLC showed that the ether layer contained only a trace amount of unreacted SLMTS (<10%). The aqueous-acetone solution was evaporated to dryness. The solid product was then placed in a desiccator over P_2O_5 overnight. The melting point of the product was 111−112 °C (dec) and the yield was 65%. No further characterization of SLMTCys was carried out. In Figure 1 are illustrated the structural formulas of SLMTCys and its deuterated analogues (**IIa**−**d**).

S-[3-(2,2,5,5-Tetramethyl-1-oxypyrrolinyl)methylthiol]-D,L-[β,β-$^2H_2$]cysteine (**IIb**) was synthesized according to the method for **IIa** except that D,L-[β,β-$^2H_2$]cysteine was used.

S-[3-(2,2,5,5-Tetramethyl-1-oxypyrrolinyl)[$^2H_2$]methylthiol]-L-cysteine (**IIc**) was synthesized according to the method for **IIa** except that **Ib** was used.

S-[3-(2,2,5,5-Tetramethyl-1-oxypyrrolinyl)[$^2H_2$]methylthiol]-D,L-[β,β-$^2H_2$]cysteine (**IId**) was synthesized according to the method for **IIa** except that **Ib** and D,L-[β,β-$^2H_2$]cysteine were used.

Wild-Type and Glu240Cys Mutant Forms of TEM-1 β-Lactamase. A detailed description for overexpression, deuterium enrichment, creation of point mutations, and purification of recombinant TEM-1 β-lactamase employed in this investigation has been published from this laboratory (*29*). Growth of engineered *Escherichia coli* BL21 (DE3) cells on ^2H_2O and sodium [$^2H_3$]acetate (3 g/L) yielded >70 mg/L of mature wt protein enriched with deuterium to levels of 88−90%, estimated by MALDI-TOF mass spectrometry (*29*). The Glu240Cys mutant was generated by application of the polymerase chain reaction (*30*), and *E. coli* BL21 (DE3) cells transformed with the mutant gene were similarly grown on perdeuterated minimal medium (*29*).

EPR and ENDOR Spectroscopy. EPR and ENDOR spectra were recorded with use of an X-band Bruker ESP 300E spectrometer equipped with a TM_{110} cylindrical cavity, Bruker ENDOR accessory, and Oxford Instruments ESR910 liquid helium cryostat, as described previously (*31*, *32*). Typical experimental conditions for ENDOR measurements were as follows: sample temperature, 20 K; microwave frequency, 9.45 GHz; incident microwave power, 2 mW; modulation frequency, 12.5 kHz; and rf modulation depth, ~8 kHz.

Spin-labeled samples (SLMTS and SLMTCys) for EPR and ENDOR studies were dissolved to a concentration of 4 × 10^{-3} M in perdeuterated solvents. Enzyme samples were prepared by treating the Glu240Cys mutant protein either with SLMTS (**Ia**) or its deuterated analogues (**Ib** and **Ic**) in 0.1 M NaCl buffered to a pH or pD 6.0 with 0.02 M PIPES. The reaction was carried out at 25 °C for 30 min by using a 10-fold excess of ligand followed by extensive dialysis against a cacodylate buffer at 4 °C. The final concentration of the chemically modified enzyme was about 2.6 × 10^{-4} M, and the enzyme was buffered to a pH or pD 7.0 with 0.02 M cacodylate in 0.1 M NaCl. All samples were stored in liquid nitrogen for spectroscopic data collection.

Molecular Modeling. The atomic numbering schemes of SLMTS and SLMTCys are shown in Figure 1. Graphics

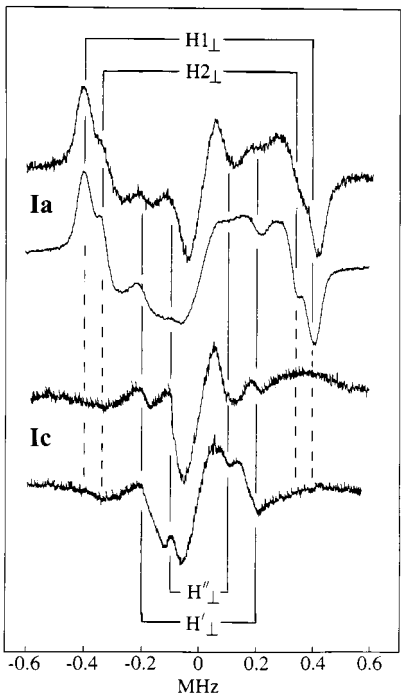

FIGURE 2: Comparison of the ENDOR spectra of SLMTS (**Ia** and **Ic**, top and bottom sets, respectively) in solvents of different dielectric constant. Samples were dissolved in perdeuterated solvents to a concentration of 4×10^{-3} M. Within each set, the upper spectrum is of **Ia** or **Ic** in [$^2H_4$]methanol while the lower spectrum is of **Ia** or **Ic** in [^{2}H]chloroform/[$^2H_8$]toluene (50:50 v/v). All spectra were collected with $\mathbf{H}_0$ setting at A. At the top of the diagram, two line pairs are identified for perpendicular hfc components of the two methylene protons. For the methyl protons, two line pairs, corresponding to two sets of perpendicular hfc components labeled $H_\perp'$ and $H_\perp''$, are identified by the stick diagram in the bottom part of the diagram. It is readily apparent that there is a change in the relative peak-to-peak amplitudes of the $H_\perp'$ and $H_\perp''$ resonance features upon change in solvent from methanol to chloroform/toluene system. This change is seen in both sets of spectra; however, the specific deuteration at the methylene and at the vinyl proton in the spin-label oxypyrrolinyl ring in **Ic** allow the change in intensity of the methyl resonance features to be more readily visually quantified. The abscissa measures the observed ENDOR shift (observed frequency of the ENDOR absorption feature minus the free proton Larmor frequency of ~14.33 MHz).

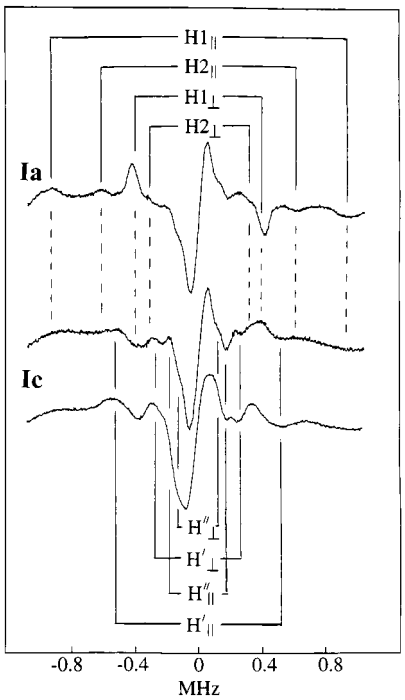

FIGURE 3: Comparison of ENDOR spectra of SLMTS in solvents of high and low dielectric constant. The top ENDOR spectrum is of **Ia** in [$^2H_4$]methanol, while the bottom set of spectra are of **Ic** in [$^2H_4$]methanol (upper spectrum) and in [^{2}H]chloroform/[$^2H_8$]toluene (50:50 v/v) (lower spectrum). All spectra were collected with $\mathbf{H}_0$ setting at B. At the top of the diagram, four line pairs are identified for parallel and perpendicular hfc components of the two methylene protons, and in the bottom part of the diagram, four line pairs, corresponding to two sets of parallel and perpendicular hfc components for the methyl protons are identified in the stick diagram. The baseline in both wings with very broad features, particularly visible in the bottom set of spectra of **Ic**, is characteristic of the oxypyrrolinyl spin-label (cf. refs *12* and *28*). Other conditions are as those in Figure 2.

modeling of SLMTS, SLMTCys, and the SLMTS-reacted Glu240Cys mutant of TEM-1 β-lactamase was carried out with use of programs SYBYL (Tripos Associates, Inc., 1600 S. Hanley Road, St. Louis, MO 63144) and INSIGHT95 (Biosym Technologies, Inc., 9685 Scranton Road, San Diego, CA 92121) running on an SGI R4400 Indigo^2 workstation with Solid Impact Graphics. Atomic coordinates of SLMTS were constructed from X-ray-defined molecular fragments of 2,2,5,5-tetramethyl-1-oxypyrroline-3-carboxamide (*33*) and aryl thiosulfonic esters (*34*), applying idealized bond lengths and valence angles (*35*). Atomic coordinates of SLMTCys were similarly constructed from the model structure of SLMTS and the X-ray-defined structure of L-cystine (*36*). The atomic coordinates of TEM-1 β-lactamase (file 1BTL) were obtained from the Brookhaven Protein Data Bank (*37*). For modeling the Glu240Cys mutant of TEM-1 β-lactamase, a cysteine residue was first inserted at the 240 position with the REPLACE option of INSIGHTII, and the spin-labeled thiomethoxy (SL$-CH_2S-$) group was attached to the sulfur atom of cysteine according to the model structure of SLMTCys, as described previously (*23*). Positions of methylene and methyl hydrogen atoms were calculated according to idealized geometries (*35*) for a tetrahedral carbon with use of SYBYL.

Systematic conformational analysis was carried out for both SLMTS and SLMTCys by application of the SEARCH routine within the program package SYBYL, as previously described (*13*−*15*, *18*, *19*, *21*). For the terminal methyl group of SLMTS, we have employed the position of the geometrically averaged hydrogens to represent the $-CH_3$ group because resonances of the individual methyl protons were not resolved. Torsion angle search calculations in 2° increments were carried out for simultaneous rotation around all rotatable bonds. The effective position of the unpaired spin density of the nitroxyl group as a point dipole was applied as the reference position for distance constraints, as described earlier (*15*). The conformation of SLMTS covalently attached to Glu240Cys mutant form of TEM-1 β-lactamase was carried out within allowed intramolecular van der Waals conformational space of SLMTS and allowed intermolecular van der Waals hard sphere contacts (*38*) with active site residues of the enzyme.

RESULTS AND DISCUSSION

Angle-Selected ENDOR for Structural Analysis. Detailed descriptions of the physical basis of angle-selected ENDOR of spin-labels are found in earlier publications (*13, 20, 23*).

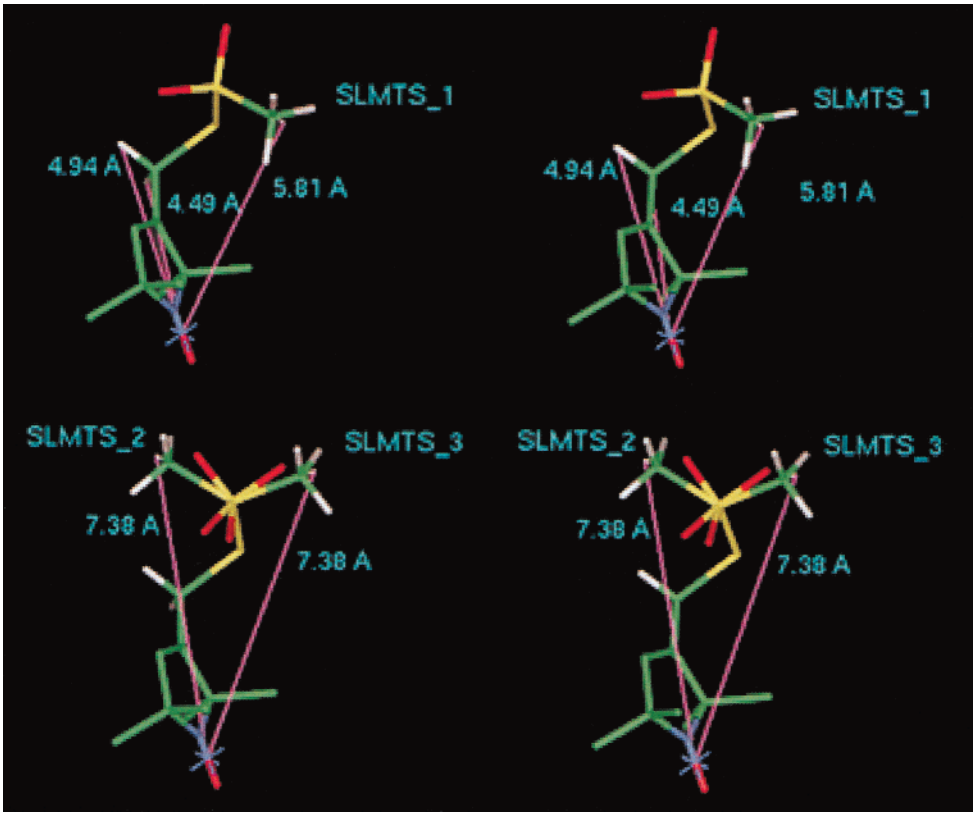

FIGURE 4: Stereo diagram of the ENDOR-determined conformations of SLMTS. The structures were drawn according to the mean dihedral angles listed in Table 3: (top) conformer **1**, which is of high population in a nonpolar solvent, and (bottom) conformers **2** and **3**, which are of high population in a polar solvent. These conformers were obtained from torsion angle search calculations constrained by ENDOR-determined electron−proton distances to the methylene and methyl protons, as listed in Table 2. The ENDOR-significant hydrogen positions with the corresponding electron−proton distances are shown in addition to the non-hydrogen atoms.

Table 2: Summary of hfc Components[a] and Estimated Electron−Proton Distances in Methyl 3-(2,2,5,5-tetramethyl-1-oxypyrrolinyl)methanethiolsulfonate

proton	$A_{\|\|}$	$A_{\perp}$	A_{iso}	$A_{\|\|}^{D}$	$A_{\perp}^{D}$	r (Å)
H1(CH_2)	1.845	0.800	0.082	1.763	−0.882	4.48 ± 0.03
H2(CH_2)	1.258	0.686	−0.038	1.296	−0.648	4.95 ± 0.03
H′(CH_3)[b]	0.820	0.396	0.009	0.811	−0.405	5.81 ± 0.05
H″(CH_3)[b]	0.391	0.200	−0.003	0.394	−0.197	7.38 ± 0.08

[a] hfc components are in units of MHz. Uncertainty in the ENDOR shift of 15−20 kHz estimated from the line width of ENDOR absorption is included as the uncertainty in the calculation of electron−proton distances. [b] For methyl protons, two sets of perpendicular hfc components, labeled as H′(CH_3) and H″(CH_3), are observed and are assigned to two conformers: the resonance features H′ refers to one conformation of the side chain as a species of high population in a nonpolar solvent, and the resonance feature H″ refers to the other conformation of the side chain as a species of high population in a polar solvent.

Table 3: Values of Dihedral Angles of the ENDOR-Constrained Conformation of Methyl 3-(2,2,5,5-tetramethyl-1-oxypyrrolinyl)methanethiolsulfonate

	τ (deg)		
dihedral angle	conformer **1**[a]	conformer **2**[b]	conformer **3**[b]
[C(3′)═C(2′)−C(1)−S(1)]	102 ± 2	102 ± 4	102 ± 4
[C(2′)−C(1)−S(1)−S(2)]	−74 ± 4	−85 ± 20	−85 ± 20
[C(1)−S(1)−S(2)−C_M]	108 ± 4	−61 ± 25	157 ± 25

[a] Conformer **1** was found from torsion angle search calculations based on the ENDOR-determined distance constraint to H′(CH_3) of 5.81 ± 0.05 Å in addition to the two methylene protons (predominant conformer in a nonpolar, aprotic solvent). [b] Conformers **2** and **3** were found from torsion angle search calculations based on the ENDOR-determined distance constraint to H″(CH_3) of 7.38 ± 0.08 Å in addition to the two methylene protons (predominant conformers in a polar solvent).

We briefly review the basic geometrical relationships underlying the orientation dependence of hf couplings of protons with the unpaired electron of the nitroxyl group with respect to the setting of the static (laboratory) magnetic field $\mathbf{H}_0$ to facilitate the presentation and discussion of ENDOR spectra. The hf interactions are governed by the $\mathbf{g}_e$ tensor, which defines the principal axes of the interactions of the unpaired electron, and the **A** tensor, which correspondingly describes the principal hyperfine axes of a proton. In spin-labels, the axes of the $\mathbf{g}_e$ and **A** tensors are essentially coincident and g anisotropy is very small. The g_z component of $\mathbf{g}_e$ is coincident with the molecular z axis and, therefore, perpendicular to the molecular x,y plane. The low-field absorption feature of the EPR spectrum arises from those molecules for which the g_z component is coincident with the static magnetic field $\mathbf{H}_0$. Microwave power saturation that drives the transitions of the unpaired electron then selects perpendicularly oriented molecules for monitoring nuclear resonance transitions with resultant "single crystal-like spectra" (*12*, *13*, *39*, *40*). We have termed this condition "setting A". On the other hand, microwave saturation of the intense central feature of the EPR spectrum selects molecules of all orientations. This is termed "setting B".

For setting A, a proton in the plane of the spin-label gives rise to the perpendicular hf interaction $A_{\perp}$ while a proton located on or near the molecular z axis gives rise to the parallel hf interaction $A_{\|}$. On the other hand, for setting B of the laboratory magnetic field, an axially located proton gives

Scheme 3

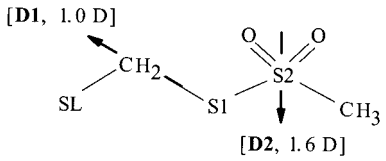

rise to a perpendicular interaction $A_\perp$ while a proton in the molecular plane gives rise to both parallel ($A_\parallel$) and perpendicular ($A_\perp$) interactions (*12*−*23*). This differential appearance of parallel and perpendicular hf couplings dependent on orientation of the spin-label with respect to the (static) laboratory magnetic field $\mathbf{H}_0$ provides a diagnostic signature for assigning the relative position of the detected magnetic nucleus according to the axes of the $\mathbf{g}_e$ tensor (*12*−*14*, *20*, *22*, *23*). In addition, of critical diagnostic importance is that the ENDOR splitting for the perpendicular hf interaction $A_\perp$ is to first-order independent of the setting of the magnetic field $\mathbf{H}_0$, while the ENDOR splitting for the parallel interaction $A_\parallel$ varies and passes through a maximum value when $\mathbf{H}_0$ reaches the canonical orientation corresponding to the principal hfc component (*13*, *20*, *40*). Assignment of resonance features in this investigation is based on these physical relationships and confirmed through experiment.

By measuring the energy of the electron−nucleus hf interaction *A*, the separation between the unpaired electron of the nitroxyl group (*15*) and each ENDOR-active nucleus can be estimated according to eq 1. In this relationship, the *g* values represent the electron and nuclear *g* factors, the β values represent the electron and nuclear Bohr magneton, respectively, *h* is the Planck constant, *r* is the electron−nucleus distance, α represents the angle between the static magnetic field $\mathbf{H}_0$ and the electron−nucleus position vector $\mathbf{r}$, and A_{iso} is the first-order isotropic hfc due to the Fermi contact interaction.

$$A = \frac{\mathbf{g}_N|\beta_N|\mathbf{g}_e|\beta_e|}{hr^3}(3\cos^2\alpha - 1) + A_{iso} \qquad (1)$$

The observed ENDOR shifts according to eq 1 correspond to the principal hfc components $A_\parallel$ and $A_\perp$ with values of 0° for the dipolar angle α for parallel hf interactions and 90° for perpendicular hf interactions, respectively. We have shown through ENDOR and TRIPLE spectroscopy that $A_\parallel > 0 > A_\perp$ for nitroxyl spin-labels (*41*). Because the value of A_{iso} can be estimated according to the constraint $(A_\parallel + 2A_\perp) = 3A_{iso}$, the dipolar hfc components $A_\parallel^D$ and $A_\perp^D$ representing the first right-hand term of eq 1 are then obtained by subtracting A_{iso} from the observed values of $A_\parallel$ and $A_\perp$. In this manner, the electron−nucleus separation *r* can be estimated directly from the hf couplings identified in the spectrum. For nuclei for which $r \geq 5$ Å, the isotropic contribution is negligibly small. We can then use the observed hfc components directly to estimate electron−nucleus distances. The validity of this approximation has been demonstrated in numerous ENDOR studies of spin-labeled compounds, including synthetic spin-labeled substrates in catalytically competent enzyme reaction intermediates (*16*, *17*, *20*−*23*).

ENDOR Studies of SLMTS. Figure 2 illustrates proton ENDOR spectra of **Ia** and **Ic** with $\mathbf{H}_0$ at setting A. The hfc components are assigned according to the stratagem described above. The resonance features of the two methylene protons are seen only in the upper set of spectra of **Ia** and are labeled $H1_\perp$ and $H2_\perp$. The perpendicular hfc components for H1 and H2 are assigned by selective deuteration because these resonance features are absent in the spectrum of **Ic**. In Figure 2, two additional pairs of features near the free proton Larmor frequency are labeled $H_\perp'$ and $H_\perp''$. These resonance features must come from the terminal methyl protons of the methanethiolsulfonate moiety. Moreover, the relative peak-to-peak amplitudes of these two features are dependent on solvent polarity. The resonance features corresponding to $H_\perp''$ are much more intense in a polar solvent such as MeOH, while the features corresponding to $H_\perp'$ are more intense in a nonpolar solvent such as chloroform/toluene (50:50 v/v). This change is seen in both sets of spectra of **Ia** and **Ic**; however, the specific deuterium substitutions in **Ic** allow the change in intensity of the methyl resonance features to be more easily recognized. Solvent-dependent changes in the peak-to-peak amplitudes of the resonance features of methyl protons indicate the presence of at least two conformers differing in their electron−proton distances.

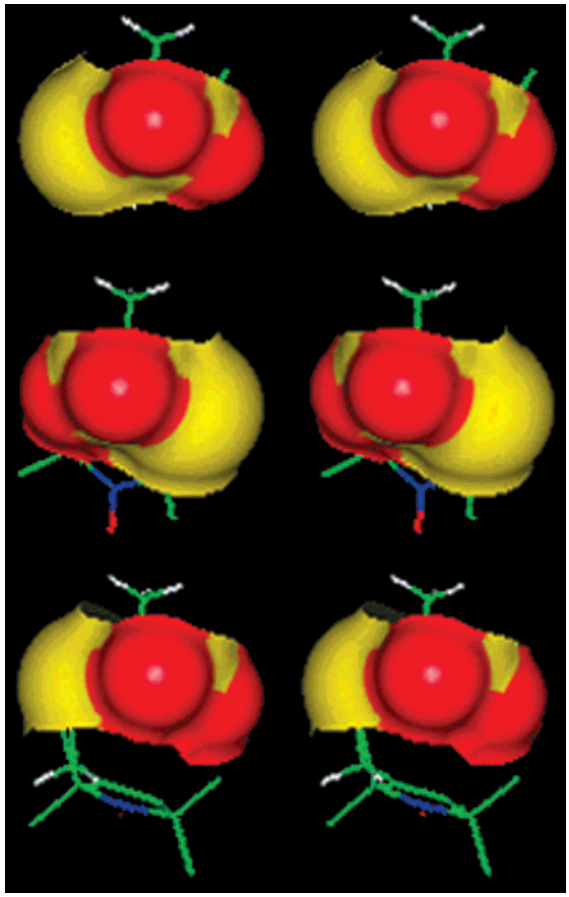

FIGURE 5: Comparison of the solvent accessible surface of the $-SSO_2-$ moiety of SLMTS in conformers **1**−**3** (top-to-bottom order). For this comparison, the $-SSO_2-$ moiety is shown for each conformer to illustrate its relative orientation of the oxypyrrolinyl ring. It is seen that, in conformers **1** and **2**, steric access of solvent molecules to the $-SSO_2-$ moiety is not hindered by atoms of the oxypyrrolinyl ring, while in conformer **3** access of solvent to the sulfur atoms is decreased. For a probe radius of 1.4 Å, the fractional contact area of the $-SSO_2-$ moiety was calculated to be 0.30, 0.29, and 0.26 of the total molecular contact area for conformers **1**−**3**, respectively. The oxygen atoms of $-SSO_2-$ moiety are colored red while the sulfur atoms are rendered yellow.

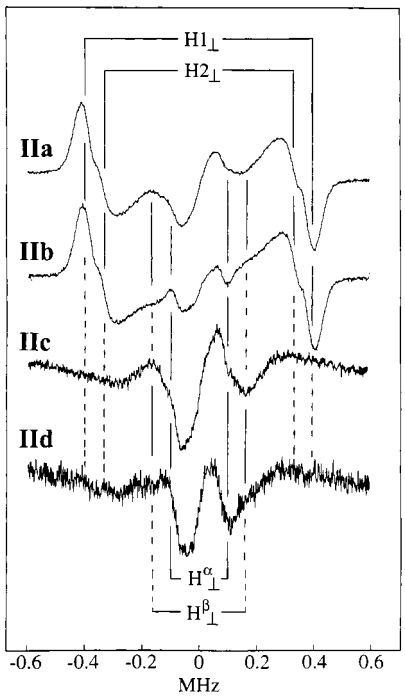

FIGURE 6: ENDOR spectra of SLMTCys in [$^2H_4$]methanol with $\mathbf{H}_0$ setting at A. At the top of the diagram, two line pairs are identified for perpendicular hfc components of the two methylene protons, labeled H1$_\perp$ and H2$_\perp$. For H$^\alpha$ and H$^{\beta1,2}$ of the cysteine side chain, two line pairs corresponding to their perpendicular hfc components are identified by the stick diagram in the bottom part of the diagram, labeled H$^\alpha{}_\perp$ and H$^\beta{}_\perp$. The dashed lines indicate the absence of proton resonance features in ENDOR spectra that are observed in **IIa** but not in specifically deuterated analogues. In this diagram, the resonance features for H$^{\beta1}$ and H$^{\beta2}$ are not clearly resolved; therefore, the broad, overlapping feature is labeled only as H$^\beta{}_\perp$. However, by data collection at an expanded scale, we have been able to show that the two distinct perpendicular hfc components of H$^{\beta1}$ and H$^{\beta2}$ are present only in spectra of **IIa** and **IIc** and are separated by 40 kHz. The values of the hfc components of H$^{\beta1}$ and H$^{\beta2}$ are listed in Table 4. Other conditions are as in Figure 2.

Table 4: Summary of hfc Components[a] and Estimated Electron−Proton Distances in *S*-[3-(2,2,5,5-Tetramethyl-1-oxypyrrolinyl)methylthiol]-L-cysteine

proton	$A_\parallel$	$A_\perp$	A_{iso}	$A_\parallel^D$	$A_\perp^D$	r (Å)
H1(CH_2)	1.835	0.785	0.088	1.747	−0.873	4.49 ± 0.03
H2(CH_2)	1.285	0.687	−0.030	1.315	−0.657	4.93 ± 0.03
H$^{\beta1}$		0.280			−0.280	6.55 ± 0.07[b]
H$^{\beta2}$		0.194			−0.194	7.41 ± 0.10[b]
H$^\alpha$	0.345	0.174	−0.001	0.346	−0.173	7.71 ± 0.08

[a] hfc components are in units of MHz. Uncertainty in the ENDOR shift of 15−20 kHz estimated from the line width of ENDOR absorption is included as the uncertainty in the calculation of electron−proton distances. [b] Because the isotropic contributions of distant protons (≥5 Å) are vanishingly small, we have calculated the values of r for the two β protons of cysteine from their principal perpendicular hfc components alone.

Figure 3 compares ENDOR spectra of SLMTS in polar and nonpolar solvents with $\mathbf{H}_0$ at position B of the EPR spectrum. In addition to the perpendicular hfc components of the methylene and methyl protons identified in Figure 2, the resonance features corresponding to the parallel hfc components are also seen and assigned on the basis of angle-selected ENDOR and selective deuteration. In Table 2, we have summarized the observed values of the parallel and perpendicular hfc components of the methylene and methyl protons. The detection of only two pairs of resonance features for each proton requires that the observed ENDOR splittings correspond to axially symmetric principal hfc components. In Table 2, we have also listed the values of isotropic and dipolar hfc components for each proton together with corresponding electron−proton separations r calculated on the basis of the dipolar eq 1.

Table 5: Values of Dihedral Angles of the ENDOR-Constrained Conformations of *S*-[3-(2,2,5,5-Tetramethyl-1-oxypyrrolinyl)methylthiol]-L-cysteine

	τ (deg)		
dihedral angle	conformer **1**[a]	conformer **2**[a]	X-ray[b]
[C(3′)═C(2′)−C(1)−S(1)]	96 ± 5	96 ± 5	−107
[C(2′)−C(1)−S(1)−S$^\gamma$]	−55 ± 10	−65 ± 10	81
[C(1)−S(1)−S$^\gamma$−C$^\beta$]	−80 ± 15	160 ± 15	103
[S(1)−S$^\gamma$−C$^\beta$−C$^\alpha$]	−155 ± 15	60 ± 15	163
[S$^\gamma$−C$^\beta$−C$^\alpha$−N]	−135 ± 30	180 ± 30	−62

[a] Conformers **1** and **2** of the spin-labeled methylthiol-L-cysteine were found from torsion angle search calculations based on the ENDOR-determined distance constraints to H$^\alpha$, H$^{\beta1}$, H$^{\beta2}$, and two methylene protons listed in Table 4. [b] Values of dihedral angles of SLMTCys in the spin-labeled Val75Cys mutant form of T4 lysozyme were obtained from the X-ray-defined structure (*11*). Atomic coordinates were provided by W. L. Hubbell (personal communication).

Conformation of SLMTS. To assign the conformation of SLMTS, we have carried out a conformational search of the torsion angles for rotation around the C(2′)−C(1), C(1)−S(1), S(1)−S(2), and S(2)−C_M bonds (see the atomic numbering scheme in Figure 1) within van der Waals hard sphere limits (*38*), using ENDOR-determined electron−proton distances listed in Table 2 as constraints. ENDOR results indicated at least two conformers of SLMTS of which the relative populations were dependent on solvent polarity. Therefore, in addition to the electron−nucleus distances to the methylene protons, we have correspondingly applied two different ENDOR distance constraints: (i) the electron−proton distance of 5.81 ± 0.05 Å to the geometrically averaged position of the methyl protons, labeled H′(CH_3); and (ii) the electron−proton distance of 7.38 ± 0.08 Å to the methyl protons, labeled H″(CH_3). The ENDOR data in the first set of calculations, corresponding to the SLMTS molecule in chloroform/toluene, limit the number of conformations within van der Waals space to a very small range, resulting in a nearly unique conformation of the methylmethanethiolsulfonate side chain with respect to the spin-label moiety. However, for the molecule in MeOH, two regions of conformational space were found compatible with the ENDOR distance constraints. In Table 3, we have summarized the values of dihedral angles for the three conformers, and in Figure 4, we have illustrated the molecular structures of the three ENDOR-compatible conformations of SLMTS. These structures correspond to the mean values of dihedral angles listed in Table 3. It is seen that the three structures differ primarily according to the relative orientation of the CH_3−S− group with respect to the spin-label moiety across the S(1)−S(2) bond.

Conformer **1** is of high population in chloroform/toluene but is of low population in MeOH. The opposite obtains for conformers **2** and **3**. Because the freezing temperature of both solvent systems employed in this investigation is approximately −100 °C, the difference in conformer population cannot be ascribed to a temperature-dependent equilib-

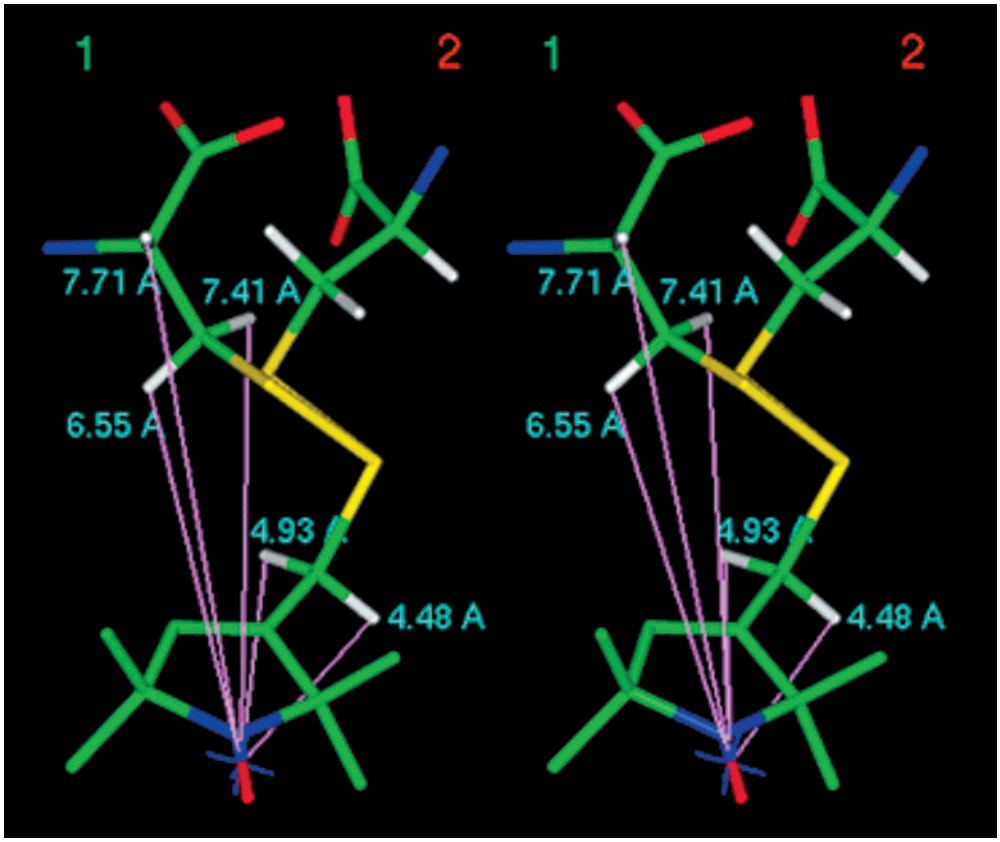

FIGURE 7: Stereo diagram of the ENDOR-determined conformations of SLMTCys. The two conformers, labeled **1** and **2**, were obtained from torsion angle search calculations constrained by ENDOR-determined electron−proton distances to the methylene protons, H^{α}, $H^{\beta 1}$, and $H^{\beta 2}$, listed in Table 4. The ENDOR-significant hydrogen positions with the corresponding electron−proton distances are shown in addition to non-hydrogen atoms.

rium. To explain the origin of the solvent dependence of conformer populations, we suggest that the interactions between the solvent and the SLMTS molecule must be of importance, in analogy to the results of earlier investigations in which the relative populations of conformers were found to be dependent on the dielectric constant of the solvent and hydrogen-bonding interactions (*14*). To this end, in Scheme 3, we show the directions and magnitudes of ground-state electric dipoles associated with the C(1)−S(1) bond and the sulfonate group, on the basis of experimentally determined values of the electric dipole moment in chemically similar compounds (*42*). The conformer dependent contribution of this dipole−dipole interaction to the potential energy of SLMTS was calculated as −1.52 kcal/mol for conformer **1**, −1.02 kcal/mol for conformer **2**, and −0.96 kcal/mol for conformer **3**. Accordingly, the Boltzmann predicted fraction of molecules in conformer **1** is 69% at room temperature, while at −100 °C this increases to ∼81% with conformers **2** and **3** accounting for 19% of the molecules in the system.

According to Scheme 3, the two dipoles in conformers **1**−**3** make angles of 101°, 79°, and 73°, respectively, changing their projection onto each other from slightly antiparallel and stabilizing to slightly parallel and destabilizing. The chloroform/toluene solvent provides little dielectric screening and at most only weak hydrogen-bonding interactions[2] that could further diminish unfavorable dipole interactions. Therefore, we conclude that the relative populations of conformers in chloroform/toluene are determined directly through Boltzmann considerations. On the other hand, because conformers **2** and **3** of higher potential energy are predominant in MeOH, hydrogen bonding of the solvent to the $-SSO_2-$ group must diminish unfavorable dipole interactions. This interaction may also favor populating one of these conformers over the other. Comparison of the fractional solvent accessible contact surface (*45*) of the $-SSO_2-$ group relative to the total surface area of each conformer, as illustrated in Figure 5, shows that (i) the sulfonate group in conformers **1** and **2** exhibits essentially equivalent contact areas and that (ii) the solvent accessibility to the S_1 atom of the $-SSO_2-$ group in conformer **3** is more restricted than in conformers **1** and **2**. The reduced area of the $-SSO_2-$ group in conformer **3** for hydrogen bonding with solvent will decrease its population in polar solvents compared to conformers **1** and **2**. On this basis, we suggest that the conformational equilibrium occurs largely between conformers **1** and **2** and that conformer **3** is likely of negligible population.

ENDOR-Constrained Conformation of SLMTCys. Figure 6 illustrates proton ENDOR spectra of SLMTCys with $\mathbf{H}_0$ at setting A. At this magnetic field setting, only one pair of resonance features is seen for each proton, as for SLMTS in Figure 2. The resonance features of the two methylene protons observed in spectra of only **IIa** and **IIb** can be assigned directly by selective deuteration and are designated $H1_{\perp}$ and $H2_{\perp}$. In Figure 6, two additional pairs of features

[2] The hydrogen atom in the chloroform molecule is acidic. Nonetheless, the energetic contribution of an aliphatic C−H···O or C−H···S hydrogen-bonding interaction is small as compared to that provided by O−H···O or O−H···S interactions (*43, 44*).

near the free proton Larmor frequency are seen and are designated $H_{\perp}^{\alpha}$ and $H_{\perp}^{\beta}$. In the spectrum of **IId**, the resonance features must come from H^{α} of the cysteine moiety because the C(1) and C^{β} atoms are deuterated. Although the resolution of resonance features for $H^{\beta 1}$ and $H^{\beta 2}$ is not apparent in this figure, their overlapping features could be assigned from spectra recorded on an expanded scale (data not shown). While the parallel hfc components for H^{α} and the two methylene protons could be assigned from ENDOR spectra of correspondingly selectively deuterated analogues of SLMTCys with $\mathbf{H}_0$ at setting B (data not shown), the parallel hfc components for $H^{\beta 1}$ and $H^{\beta 2}$ were not identifiable. For this reason, estimates of their corresponding electron−nucleus distances were made only on the basis of their perpendicular hfc components. In Table 4, we have summarized the observed values of the principal hfc components of the methylene protons, H^{α}, and $H^{\beta 1}$ and $H^{\beta 2}$ of SLMTCys. We have also listed in Table 4 the values of isotropic and dipolar hfc components, and electron−proton separations (r) together with their corresponding uncertainties.

To determine the conformation of spin-labeled methylthiol-L-cysteine, we have carried out torsion angle search calculations constrained by ENDOR-determined distances as for SLMTS. The search calculations were applied for simultaneous rotation around the C(2′)−C(1), C(1)−S(1), S(1)−S^{γ}, S^{γ}−C^{β}, C^{β}−C^{α}, C^{α}−C, and C^{α}−N bonds. In Table 5, we have summarized the values of dihedral angles for the two conformers accommodated by the ENDOR constraints in Table 4. In Figure 7, we have illustrated the molecular structures of the two ENDOR-compatible conformations of SLMTCys, labeled **1** and **2**. These two structures were drawn according to the mean values of dihedral angles listed in Table 5. The two conformations of SLMTCys are nearly identical with respect to rotation about the C(2′)−C(1) and C(1)−S(1) bonds, and they exhibit similar dihedral angles to those in SLMTS. On the other hand, the structural similarity does not extend to dihedral angles with rotation around the S^{γ}−S(1), C^{β}−S^{γ}, and C^{α}−C^{β} bonds. The dihedral angle about the S^{γ}−S(1) bond in X-ray-defined structures of L-cysteine corresponds either to left-handed (−75 ± 10°) (*46*−*48*) or right-handed (75 ± 10°) chirality (*49*). The dihedral angle [C^{β}−S^{γ}−S(1)−C(1)] of conformer **1** of SLMTCys was found to be −80 ± 15° corresponding to a disulfide of left-handed chirality. In contrast, for conformer **2** of SLMTCys, the value of this dihedral angle was 160 ± 15°, differing significantly from that of classical conformations. For this reason we believe that conformer **2** of SLMTCys represents a geometrical solution accommodating the distance constraints within van der Waals conformational space but is unlikely to be populated significantly in solution.

It is of interest to point out that X-ray structures of Lys65Cys, Arg80Cys, Arg119Cys, and Val75Cys mutants of T4 lysozyme with a disulfide-linked nitroxyl spin-label side chain [>C^{α}H−$C^{\beta}H_2$−S^{γ}−S(1)-C(1)H2−(3-(2,2,5,5-tetramethyl-1-oxypyrrolinyl))] attached to the cysteine residue have been recently determined by Hubbell and co-workers (*11*). Although the conformation around the C(2′)−C(1) bond of the spin-label could not be determined in three of the mutant proteins and the oxypyrrolinyl ring was not fully identified in the electron density maps because of local structural disorder, the two dihedral angles around the C^{α}−C^{β} and C^{β}−S^{γ} bonds were clearly defined in all four structures with values ranging among all three classical conformations $g^{+}(60°)$, $g^{-}(-60°)$, and $t(180°)$.[3] Only in the structure of the Val75Cys mutant, in which the spin-label moiety is immobilized through nearest-neighbor contact interactions, was the oxypyrrolinyl ring stabilized so that all of the atoms were identified in the electron density map (*11*). Values of dihedral angles of SLMTCys in the Val75Cys mutant form of T4 lysozyme as determined by X-ray (*11*) are also listed in Table 5. The X-ray-defined structure of the spin-label attached to the cysteine side chain in the Val75Cys mutant of T4 lysozyme (*11*) is not unlike that of conformer **1** of SLMTCys in solution except for the terminal dihedral angle around the C^{β}−C^{α} bond. Values of the other four dihedral angles differ from each other only according to reflection. This is seen by the values of the dihedral angles in Table 5. They are comparable in magnitude but differ only in sign. It is important to point out here that, as in SLMTS, we have also found by ENDOR two conformations for SLMTCys around the S(1)−S^{γ} bond. However, Hubbell and co-workers did not report multiple conformers around the S(1)−S^{γ} bond of spin-labeled T4 lysozyme mutants (*11*).

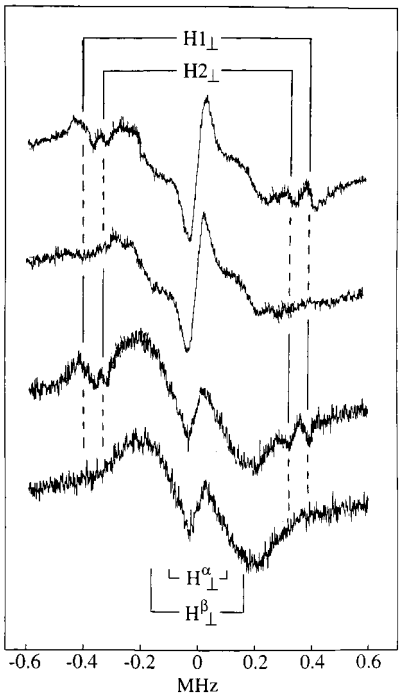

FIGURE 8: ENDOR spectra of the spin-labeled Glu240Cys mutant of TEM-1 β-lactamase with $\mathbf{H}_0$ at setting A. ENDOR spectra are shown for the following samples in top-to-bottom order: SLMTS + β-lactamase; SL[1-$^2H_2$]MTS + β-lactamase; SLMTS + perdeuterated β-lactamase; and SL[1-$^2H_2$]MTS + perdeuterated β-lactamase. The final concentration of the enzyme was 2.62×10^{-4} M, and the enzyme was buffered to a pH or pD 7.0 with 0.02 M cacodylate and 0.1 M NaCl. See Materials and Methods for a detailed description of the preparation of samples for ENDOR. At the top of the diagram, two line pairs are identified for perpendicular hfc components of the two methylene protons, labeled $H1_{\perp}$ and $H2_{\perp}$. In the lower part of the diagram, two line pairs are identified for perpendicular hfc components of H^{α}, $H^{\beta 1}$ and $H^{\beta 2}$ of the cysteine side chain and are labeled $H^{\alpha}{}_{\perp}$ and $H^{\beta}{}_{\perp}$. Other conditions are as those in Figures 2 and 6.

[3] The conventions and nomenclature used are those described by the IUPAC−IUB Commission on Biochemical Nomenclature, (1970) *Biochemistry 9*, 3471−3479.

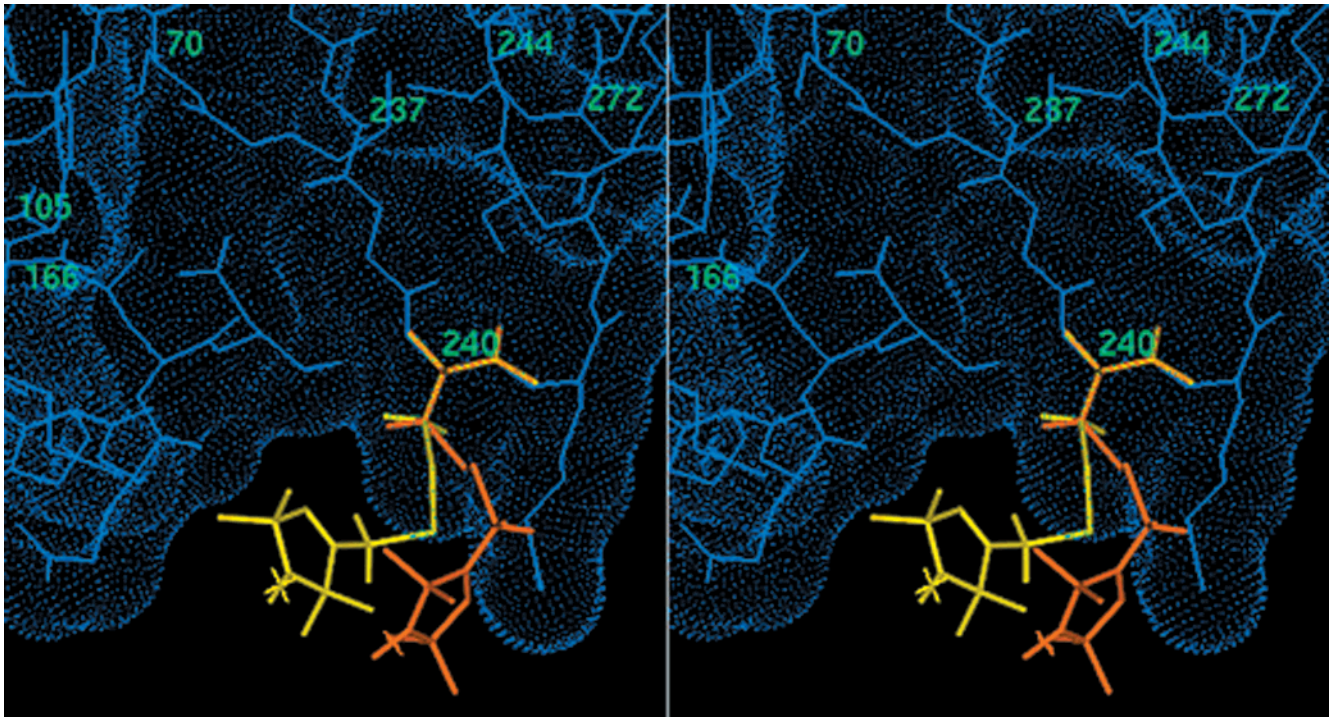

FIGURE 9: Stereo diagram of the ENDOR-determined structures of SLMTS in the active site of the Glu240Cys mutant of TEM-1 β-lactamase. The blue-dotted surface represents the calculated solvent accessible surface of the active site (*45*), and important active site residues are identified by sequence number. As seen in this diagram, the active site cleft near the spin-labeled thiomethoxy-modified side chain of residue Cys240 is not sterically restrictive. The structures of the two conformers of free spin-labeled methylthiol-L-cysteine in solution, shown in yellow and orange, respectively, for conformers **1** and **2**, are directly accommodated by the calculated solvent accessible surface and the ENDOR-determined electron−proton distances listed in Table 4. The extensive solvent exposure of the oxypyrrolinyl ring is, thus, consistent with the observation that the spin-label cysteine adduct in this instance is associated with the conformation of the free molecule.

The X-ray structure demonstrates that the conformation of the spin-labeled cysteine adduct in proteins is determined by steric contacts of nearby residues in the protein. Of interest to note from our comparison of the conformers of SLMTCys with the spin-label at position 75 in the T4 lysozyme mutant is that this site would have sterically accommodated conformer **1** but not conformer **2**. As noted by Hubbell and coworkers (*11*), the spin-label cysteine adduct is sufficiently flexible with respect to torsional changes and, therefore, is accommodated readily into binding sites in proteins with little perturbation of the protein away from its native structure.

ENDOR and Molecular Modeling of SLMTS in the Active Site of TEM-1 β-Lactamase. β-lactamases are widespread bacterial enzymes that effectively inactivate the classical β-lactam families of antibiotics and play a major role in bacterial resistance. Among the four classes (A−D), of the class A enzymes, particularly, the TEM plasmid is the most notorious because of its proven ability to readily mutate into forms capable of resisting even the newest generation of β-lactamase inhibitors. TEM-1 β-lactamase is very well characterized through X-ray crystallographic studies (*37*). We have recently reported ENDOR structural characterization of a catalytically competent acylenzyme intermediate of TEM-1 β-lactamase with a spin-labeled penicillin substrate (*23*). In that study, we have determined the positions of the cysteine residues in Met272Cys and Glu240Cys mutants through chemical modification of the cysteine residue with methylmethanethiolsulfonate (*23*). The results indicated that the position of the chemically modified residue at position 272 was essentially identical to its unmodified counterpart in the native or wild-type enzyme. On the other hand, the ENDOR results showed that the thiomethoxy modified side chain of Cys240 in the Glu240Cys mutant was slightly shifted from the X-ray defined position of the corresponding Glu240 residue in the native enzyme (*37*). Here, we have employed SLMTS to determine its conformation when reacted with the Glu240Cys mutant of TEM-1 β-lactamase.

Figure 8 illustrates proton ENDOR spectra of the Glu240Cys mutant form of TEM-1 β-lactamase reacted with SLMTS. The two upper ENDOR spectra were recorded with fully protiated TEM-1 β-lactamase, while the two lower spectra were recorded with enzyme randomly enriched with covalent deuterium (88−90% ^{2}H) obtained by growth of genetically engineered bacteria in perdeuterated minimal medium (*29*). The resonance features of two methylene protons are assigned by selective deuteration and are labeled $H1_\perp$ and $H2_\perp$ at the top of the diagram. By comparison of these ENDOR spectra with the spectra of SLMTCys, two additional pairs of features near the free proton Larmor frequency are assigned to H^α and $H^{\beta 1}$ and $H^{\beta 2}$ of Cys240 and are labeled $H_\perp{}^\alpha$ and $H_\perp{}^\beta$ at the bottom of the diagram. While these ENDOR features are similar to the spectra of SLMTCys in solution, the intense matrix ENDOR absorption observed in the two upper spectra, not observed for SLMTCys under similar solvent conditions, indicate that SLMTS is covalently attached to the mutant Cys240 residue. The observed hfc components yield essentially identical electron−proton distances to those of SLMTCys in solution listed in Table 4.

Figure 9 illustrates the spin-labeled thiomethoxy group covalently attached to Cys240 in the active site of TEM-1 β-lactamase modeled on the basis of X-ray defined atomic coordinates of the free enzyme (*37*). The residues to define the active site surface were selected as described earlier (*23*).

Both conformers of the spin-label moiety in Figure 7 are accommodated by the calculated solvent accessible surface (*45*) of active site residues in the Glu240Cys mutant of TEM-1 β-lactamase. The Cys240 side chain in the mutant enzyme is probably shifted upon reaction with SLMTS, as with methylmethanethiolsulfonate found in our earlier study (*23*); however, there is no spectroscopic signal that allows us to measure the change in position. As seen in Figure 9, the active site cleft near residue 240 is not sterically restrictive, and both conformers of the spin-labeled thiomethoxy moiety determined by ENDOR for the free molecule in solution are sterically accommodated within the active site of the enzyme. We can thus conclude that chemical modification of residues in this region of the active site with SLMTS has not evoked large changes in the structure of TEM-1 β-lactamase.

CONCLUDING REMARKS

Site-directed spin-labeling has been heretofore applied to determine topology in membrane proteins, to locate helical and β-sheet regions in proteins, and to follow protein conformational changes, only by EPR spectroscopy. By using a thiolsulfonate derivative with the unsaturated five-membered oxypyrrolinyl ring, as shown in Scheme 1, we have demonstrated that the spin-label probe is indeed suitable as a structural probe for ENDOR spectroscopy. The results presented here demonstrate the usefulness of ENDOR as an accurate, noncrystallographic method for determining the structures of molecules in (frozen) solution. In this investigation, we have provided detailed three-dimensional structures of SLMTS, spin-labeled methylthiol-L-cysteine, and of SLMTS bound in the active site of the Glu240Cys mutant of TEM-1 β-lactamase. Despite the usefulness of SLMTS as a paramagnetic and structural probe to investigate protein structure and dynamics, the molecular structure and conformation of the molecule in solution has not been determined heretofore. The results of this study show that ENDOR spectroscopy of nitroxyl spin-labels is most incisively applied to problems requiring precise definition of the detailed local structure of molecules in solution. Coupled with biosynthetic methods for random or site-specific deuteration of proteins, spin-labeled cysteine mutagenesis can be advantageously applied with ENDOR spectroscopy to determine structure and conformation of biological macromolecules.

ACKNOWLEDGMENT

We thank Professor Wayne Hubbell for personal communication of X-ray coordinates and Ms. Jennifer E. Hofer for assistance in chemical synthesis.

SUPPORTING INFORMATION AVAILABLE

Two torsion angle maps: (a) for rotation around the C(2′)−C(1) and C(1)−S(1) bonds, and (b) S(1)−S^{γ} and C(1)−S(1) bonds of SLMTCys, showing conformational space allowed by only nonbonded van der Waals contacts and by ENDOR-determined distance constraints along with vdW contacts and comparing them with the conformation determined by X-ray diffraction studies. This material is available free of charge via the Internet at http://pubs.acs.org.

REFERENCES

1. Hubbell, W. L., Gross, A., Langen, R., and Leitzov, M. A. (1998) *Curr. Opin. Struct. Biol. 8*, 649−656.
2. Wang, Q., Voss, J., Hubbell, W. L., and Kaback, H. R. (1998) *Biochemistry 37*, 4910−4915.
3. Hustedt, E. J., and Beth, A. H. (1996) *Biochemistry 35*, 6944−6954.
4. Perozo, E., Cortes, D. M., and Cuello, L. G. (1999) *Science 285*, 73−78.
5. Perozo, E., Cortes, D. M., and Cuello, L. G. (1998) *Nat. Struct. Biol. 5*, 459-469.
6. Millhauser, G. L. (1992) *Trends Biochem. Sci. 17*, 448−452.
7. Claciano, L. J., Escobar, W. A., Millhauser, G. L., Miick, S. M., Rubaloff, J., Todd, P., and Fink, A. L. (1993) *Biochemistry 32*, 5644−5649.
8. Ostap, E. M., Barnett, V. A., and Thomas, D. D. (1995) *Biophys. J. 69*, 177−188.
9. Baker, J. E., Brust-Mascher, I., Ramachandran, S., LaConte, L. E. W., and Thomas, D. D. (1998) *Proc. Natl. Acad. Sci. U.S.A.* 95, 2944−2949.
10. Smith, D. J., Maggio, E. T., and Kenyon, G. L. (1975) *Biochemistry 14*, 766−771.
11. Langen, R., Joon-Oh, K., Cascio, D., and Hubbell, W. L. (2000) *Biochemistry 39*, 8396−8405.
12. Wells, G. B., and Makinen, M. W. (1988) *J. Am. Chem. Soc. 110*, 6343−6352.
13. Mustafi, D., Sachleben, J. R., Wells, G. B., and Makinen, M. W. (1990) *J. Am. Chem. Soc. 112*, 2558−2566.
14. Wells, G. B., Mustafi, D., and Makinen, M. W. (1990) *J. Am. Chem. Soc. 112*, 2566−2574.
15. Mustafi, D., Joela, H., and Makinen, M. W. (1991) *J. Magn. Reson. 91*, 497−504.
16. Wells, G. B., Mustafi, D., and Makinen, M. W. (1994) *J. Biol. Chem. 269*, 4577−4586.
17. Mustafi, D., and Makinen, M. W. (1994) *J. Biol. Chem. 269*, 4587−4595.
18. Mustafi, D., and Makinen, M. W. (1995) *J. Am. Chem. Soc. 117*, 6739−6746.
19. Mustafi, D., Knock, M. M., Shaw, R. W., and Makinen, M. W. (1997) *J. Am. Chem. Soc. 119*, 12619−12628.
20. Makinen, M. W., Mustafi, D., and Kasa, S. (1998) in *Biological Magnetic Resonance, Spin-Labeling IV: The Next Millennium* (Berliner, L. J., Ed.) Vol. 14, pp 181−249, Plenum, New York.
21. Jiang, F., Tsai, S. W., Chen, S., and Makinen, M. W. (1998) *J. Phys. Chem. 102*, 4619−4627.
22. Makinen, M. W. (1998) *Spectrochim. Acta A54*, 2269−2281.
23. Mustafi, D., Sosa-Peinado, A., and Makinen, M. W. (2001) *Biochemistry 40*, 2397−2409.
24. Rozantsev, E. G. (1972) *Free Nitroxyl Radicals*, Chapter 9, pp 203−206, Plenum, New York.
25. Brown, H. C., and Rao, B. C. S. (1958) *J. Am. Chem. Soc. 80*, 5377−5380.
26. Kenyon, G. L., and Bruice, T. W. (1977) *Methods Enzymol. 47*, 407−431.
27. Berliner, L. J., Grunwald, J., Hankovszky, H. O., and Hideg, K. (1982) *Anal. Biochem. 119*, 450−455.
28. Mustafi, D., Wells, G. B., Joela, H., and Makinen, M. W. (1990) *Free Radical Res. Commun. 10*, 95−101.
29. Sosa-Peinado, A., Mustafi, D., and Makinen, M. W. (2000) *Prot. Expres. Purific. 19*, 235−245.
30. Ho, S. N., Hunt, H. D., Horton, R. M., Pullen, J. K., and Pease, L. R. (1989) *Gene 77*, 51−59.
31. Mustafi, D., and Nakagawa, Y. (1994) *Proc. Natl. Acad. Sci. U.S.A. 91*, 11323−11327.
32. Jiang, F. S., and Makinen, M. W. (1995) *Inorg. Chem. 34*, 1736−1744.
33. Turley, J. W., and Boer, F. P. B. (1972) *Acta Crystallogr. B28*, 1641−1644.
34. Caputo, R., Palumbo, G., Nardelli, M., and Pelizzi, G. (1984) *Gazz. Chim. Ital. 114*, 421−430.
35. Kennard, O. (1968) in *International Tables for X-ray Crystallography* (MacGillavry, C. H., Rieck, G. D., Eds.), Vol. 3, Section 4.1, pp 257−274, Kynoch Press, Birmingham, U.K.
36. Rajeswaran, M., and Parthasarathy, R. (1985) *Acta Crystallogr. C41*, 726−728.

37. Jelsch, C., Maury, L., Masson, J. M., and Samama, J. P. (1993) *Proteins*: *Struct., Funct., Genet. 16*, 364−383.
38. Iijima, H., Dunbar, J. B. Jr., and Marshall, G. R. (1987) *Proteins*: *Struct., Funct., Genet. 2*, 330−339.
39. Rist, G. H., and Hyde, J. S. (1970) *J. Chem. Phys. 52*, 4633−4643.
40. Hurst, G. C., Henderson, T. A., and Kreilick, R. W. (1985) *J. Am. Chem. Soc. 107*, 7294−7299.
41. Mustafi, D., and Joela, H. (1995) *J. Phys. Chem. 99*, 11370−11375.
42. Smyth, C. P. (1955) *Dielectric Behavior and Structure*, Chapter 9, pp 260−311, McGraw-Hill, New York.
43. Poland, D., and Scheraga, H. A. (1967) *Biochemistry 6*, 3791−3800.
44. Van Wart, H. E., and Scheraga, H. A. (1977) *Proc. Natl. Acad. Sci. U.S.A. 74*, 13−17.
45. Lee, B., and Richards, F. M. (1971) *J. Mol. Biol. 55*, 379−400.
46. Chaney, M. O., and Steinrauf, L. K. (1968) *Acta Crystallogr. B24*, 1564−1567.
47. Yakel, H. L., and Hughes, E. W. (1954) *Acta Crystallogr. 7*, 291−297.
48. Peterson, J., Steinrauf, L. K., and Jensen, L. H. (1960) *Acta Crystallogr. 13*, 104−109.
49. Chaney, M. O., and Steinrauf, L. K. (1974) *Acta Crystallogr. B30*, 711−716.

BI010539P